Available online at www.sciencedirect.com
ScienceDirect
Journal of Power Sources 178 (2008) 561–574
JOURNAL OF POWER SOURCES
www.elsevier.com/locate/jpowsour

New inorganic–organic proton conducting membranes based on Nafion® and $[(ZrO_2)\cdot(SiO_2)_{0.67}]$ nanoparticles: Synthesis vibrational studies and conductivity☆

Vito Di Noto[a,b,*,1], Matteo Piga[a], Luigi Piga[a], Stefano Polizzi[c], Enrico Negro[a]

[a] *Dipartimento di Scienze Chimiche, Università di Padova, Via Marzolo 1, I-35131 Padova (Pd), Italy*
[b] *Istituto di Scienze e Tecnologie Molecolari, ISTM-CNR c/o Dipartimento di Scienze Chimiche, Via Marzolo 1, I-35131 Padova (Pd), Italy*
[c] *Dipartimento di Chimica Fisica, Università di Venezia, Via Torino 155, I-30170 Mestre (Ve), Italy*

Received 14 July 2007; received in revised form 12 September 2007; accepted 16 September 2007
Available online 21 September 2007

Abstract

In this report is described the preparation of six nanocomposite membranes of formula $\{Nafion/[(ZrO_2)\cdot(SiO_2)_{0.67}]_{\Psi_{ZrO_2}}\}$ with Ψ_{ZrO_2} ranging from 0 to 1.79 based on Nafion® and $[(ZrO_2)\cdot(SiO_2)_{0.67}]$ nanofiller. Morphology investigations carried out by SEM measurements indicate that the composition of membranes is asymmetric. Indeed, with respect to the direction of the films after casting procedure, the top side (A-side) and bottom side (B-side) present a different nanofiller concentration. The concentration of nanofiller increases gradually from A to B side. The membranes present thicknesses ranging from 170 to 350 nm and are studied by FT-IR ATR and micro-Raman measurements.

The vibrational investigations permit us to reveal that: (a) the hydrophobic polytetrafluoroethylene (PTFE) domains of Nafion® are composed of a mixture of polymer chains with 15_7 and 10_3 helical conformations; (b) the concentration of chains with 10_3 helical conformation depends on the nanofiller concentration and is much higher in side A; (c) six different water domains are present in bulk membranes which are singled out as I, I^I, II, II^I, III and IV; (d) water uptake of membranes is correlated to the conformational transition $10_3 \rightarrow 15_7$ of PTFE chains occurring in hydrophobic domains of Nafion®. The conductivity of $\{Nafion/[(ZrO_2)\cdot(SiO_2)_{0.67}]_{\Psi_{ZrO_2}}\}$ was determined by analyzing the complex conductivity plots measured in the frequency and temperature range of 10^{-2} Hz–10 MHz and 5–155 °C, respectively. Interestingly, the $\{Nafion/[(ZrO_2)\cdot(SiO_2)_{0.67}]_{\Psi_{ZrO_2}}\}$ nanocomposite membranes with $\Psi_{ZrO_2} = 0.313$ and 0.534 showed values of conductivity of 4.3×10^{-2} S cm^{-1} at 135 °C and of 3.5×10^{-2} S cm^{-1} at 115 °C, respectively.

Keywords: Hybrid inorganic–organic proton conducting membranes; Nafion®; Fuel cells; Scanning electron microscopy; Micro-Raman spectroscopy; FT-IR ATR spectroscopy

1. Introduction

Perfluorinated polymer electrolytes such as Nafion®, Aciplex, Flemion and Dow membranes are crucial materials for the development of polymer electrolyte membrane fuel cells (PEMFCs) and direct methanol fuel cells (DMFCs) [1,2]. In these devices, the hydrated condition of the protonated form of a proton conducting membrane (PEM) is a critical parameter to control in order to obtain PEMFCs and DMFCs with a high performance and durability [3].

Organic-inorganic composite membranes based on Nafion® and inorganic micrometer to nanometer size fillers have been intensively explored and remain one of the most interesting routes in the preparation of promising electrolytes for application in fuel cells [4–12]. Thus, Nafion® membranes doped with: (a) heteropolyacids, such as phosphotungstic acid (PTA), allowed to obtain fuel cells with high performance at lower relative humidity (RH) and elevated temperature (ca. 120 °C); (b) hygroscopic oxides, such as SiO_2, TiO_2, ZrO_2, Al_2O_3 and oth-

☆ Oral contribution presented at the PBFC-2007 conference.
* Corresponding author. Tel.: +39 049 827 5229; fax: +39 049 827 5229.
E-mail address: vito.dinoto@unipd.it (V. Di Noto).
[1] Active ECS and ISE member.

0378-7753/$ – see front matter © 2007 Elsevier B.V. All rights reserved.
doi:10.1016/j.jpowsour.2007.09.043

ers, were proposed with the aim to increase the water uptake of the membranes and to decrease the humidification requirements of PEMFCs [4–12].

To date, the influence of chemical and physical properties of the inorganic fillers on the structure of the composite proton conducting polymer electrolytes is not well understood and prompted us to investigate Nafion® composite membranes systematically under varying conditions [4,13,14]. Thus, the effects of silica concentration in [Nafion/$(SiO_2)_x$] nanocomposite membranes with $0 \leq x \leq 15$ wt% has been studied demonstrating that the inorganic filler and the four different water species domains embedded in bulk membranes affect the dynamic relaxations of Nafion® and thus, the material conductivity [12]. In addition, it was shown that the formation of dynamic cross-links $SiO_2 \cdots HSO_3-$ in hydrophilic polar clusters influences the chain dynamics of hydrophobic fluorocarbon domains of the host material. Further investigations were performed on the [Nafion/$(M_xO_y)_n$] membranes with M=Ti, Zr, Hf, Ta and W and $n = 5$ wt% [15]. Particularly, by vibrational spectroscopy it was demonstrated that fluorocarbon domains of [Nafion/$(M_xO_y)_n$] materials consist mostly of chains with helical conformation 15_7 with a smaller amount of 10_3 helices [15]. The concentration of 10_3 helical chains depends on the type of metal oxide used in the preparation of the composite membrane. Furthermore, it was revealed that the amount of each of the four water domains detected in the bulk membranes depends on the acidity of M_xO_y oxocluster. Particularly, it was observed that the mechanical, thermal and dynamic characteristics of Nafion® host polymer depend on the concentration in bulk material of dynamic cross-links, $R–SO_3H \cdots M_xO_y \cdots HSO_3–R$, which are responsible for the good thermal, mechanical and electrical stability of the materials. In continuation of our efforts to develop new Nafion®-based nanocomposite materials with improved performance and to elucidate systematically the effect of inorganic fillers on the chemical and physical properties of membranes, here we investigated the influence on membrane structural characteristics of: (a) ZrO_2 nanofillers covered with a SiO_2 layer; (b) nanofiller concentration; (c) Nafion®-nanofiller interactions.

These studies were carried out by preparing seven nanocomposite membranes of formula {Nafion/[$(ZrO_2)\cdot(SiO_2)_{0.67}$]$_{\Psi_{ZrO_2}}$} with $0 \leq \Psi_{ZrO_2} \leq 1.79$, where [$(ZrO_2)\cdot(SiO_2)_{0.67}$] is a ZrO_2 nanoparticle core covered with a thin layer of SiO_2. This aim was pursued by studying seven different films prepared by solvent casting procedure at 100 °C from a dispersion of Nafion® and [$(ZrO_2)\cdot(SiO_2)_{0.67}$] nanoparticles. The nanocomposite polymer electrolyte films were accurately characterized by scanning electron microscopy (SEM) and vibrational FT-IR ATR and micro-Raman laser spectroscopy. Vibrational investigations were performed in order to elucidate: (a) the [$(ZrO_2)\cdot(SiO_2)_{0.67}$]-Nafion® polymer interactions; (b) the water domain distributions present in bulk materials; and (c) the effect of [$(ZrO_2)\cdot(SiO_2)_{0.67}$]-Nafion® interactions on the secondary structure of fluorocarbon chains in the hydrophobic PTFE domains of membranes. Impedance measurements were performed in order to measure the conductivity dependence on temperature and composition.

2. Experimental

2.1. Reagents

Nafion® ionomer 5 wt% solution (perfluorosulfonic acid PTFE copolymer solution) with a proton exchange capacity of 0.80 meq g^{-1} (Alfa Aesar, ACS grade) was used as purchased. MO_2 nanometric oxoclusters with M=Si and Zr (Aldrich, ACS grade) were purified by standard methods [16]. The SiO_2 and ZrO_2 oxides were characterized by an average particle size of 7 and 20–30 nm, respectively and by a density of 2.2 and 5.19 g mL^{-1}, respectively. All solvents used were supplied by Aldrich and further purified by standard methods. Bidistilled/milli-Q water was used in all procedures.

2.2. Nanofiller preparation

A dimethylformamide (DMF) suspension of 2.000 g of ZrO_2 (75 wt%) and 0.650 g of SiO_2 (25 wt%) was milled for 10 h at 500 rpm in a tungsten carbide grinding jar using a planetary ball mill. The viscous solution was quantitatively transferred into a 100 mL volumetric flask and diluted with DMF. A suspension of [$(ZrO_2)\cdot(SiO_2)_{0.67}$] nanoparticles was obtained, having a concentration of ZrO_2 and SiO_2 of 0.1623 and 0.1082 M, respectively. The homogeneous precursor solution A was prepared by treating under an ultrasonic bath for 1 h a mixture prepared by

Table 1
Reagent composition and molar ratios for {Nafion/[$(ZrO_2)\cdot(SiO_2)_{0.67}$]$_{\Psi_{ZrO_2}}$} membranes.

ZrO_2 (g)	SiO_2 (g)	Nafion® (g)	x (wt% ZrO_2)	x (wt% SiO_2)	ΨZrO_2[a]	ΨSiO_2[b]	Ψ[c]	φ[d]
–	–	0.45	–	–	0	0	0	0.800
0.0139	0.0045	0.45	2.97	0.96	0.313	0.210	0.525	0.779
0.0237	0.0078	0.45	4.92	1.62	0.534	0.360	0.894	0.765
0.0445	0.0146	0.45	8.74	2.87	1.003	0.676	1.679	0.738
0.0556	0.0182	0.45	10.61	3.47	1.253	0.841	2.094	0.725
0.0672	0.0220	0.45	12.46	4.08	1.515	1.019	2.534	0.712
0.0794	0.0260	0.45	14.30	4.68	1.790	1.202	2.992	0.699

[a] $\Psi_{ZrO_2} = mol_{ZrO_2}/mol_{-SO_3H}$.
[b] $\Psi_{SiO_2} = mol_{SiO_2}/mol_{-SO_3H}$.
[c] $\Psi = (mol_{ZrO_2} + mol_{SiO_2})/mol_{-SO_3H}$.
[d] $\varphi = (meq_{Nafion} + meq_{ZrO_2} + meq_{SiO_2})/g_{Composite}$.

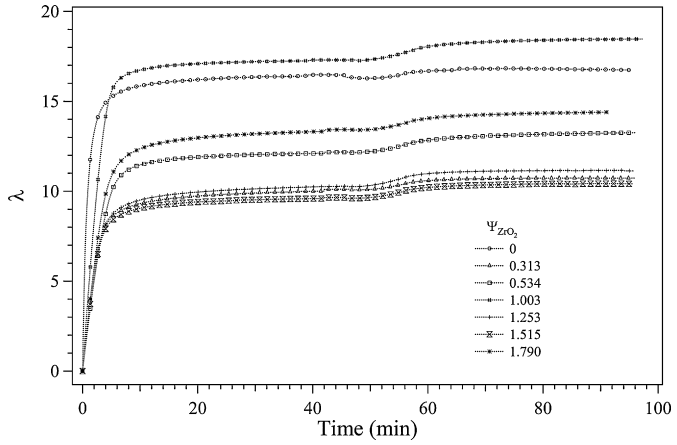

Fig. 1. λ vs. time for $\{Nafion/[(ZrO_2)\cdot(SiO_2)_{0.67}]_{\Psi_{ZrO_2}}\}$ membranes with $0 \leq \Psi_{ZrO_2} \leq 1.79$.

adding 2 mL of 30 wt% of NH_3 to a suitable amount of the above described $[(ZrO_2)\cdot(SiO_2)_{0.67}]$ suspension.

2.3. Membrane preparation

Seven $\{Nafion/[(ZrO_2)\cdot(SiO_2)_{0.67}]_{\Psi_{ZrO_2}}\}$ nanocomposite membranes, with Ψ_{ZrO_2} ranging from 0 to 1.790, have been prepared by a general solvent casting procedure as follows. A suitable amount of Nafion® (0.45 g; see Table 1) suspended in DMF and prepared as described elsewhere [12,15] was added to a suitable amount of A solution. The mixture was homogenized by a treatment in ultrasonic bath for 2 h. The resulting solution was recast in a Petri dish with a diameter of 2.5 cm, at 100 °C, for 10 h, under a hot air stream.

The resulting membranes were: (a) first, dislodged from the Petri dish by a treatment with hot milli-Q water; (b) second, partially dried under air at room temperature for 1 h; and (c) third, hot pressed at $T = 100$ °C and $p = 70$ bar for 5 min to improve their mechanical properties. The thickness of the prepared films ranged from 170 to 350 μm.

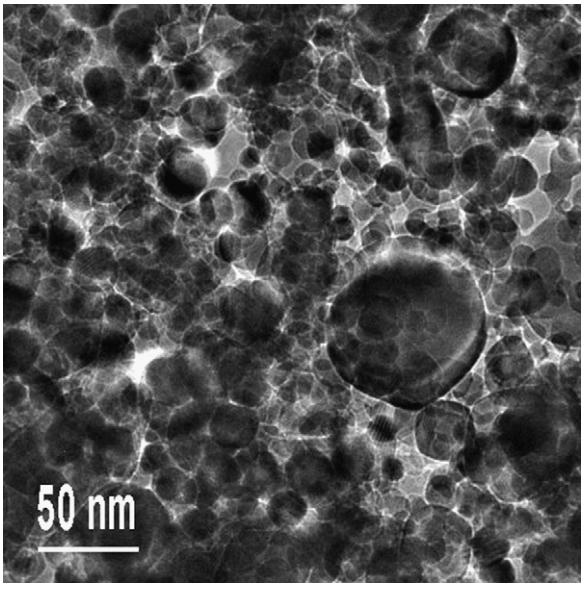

Fig. 3. TEM image of the $[(ZrO_2)\cdot(SiO_2)_{0.67}]$ nanofiller particles.

2.4. Membrane activation

The purification and activation of prepared hybrid membranes were carried out as follows. First, the composite film was heated at 80 °C in bidistilled water for 1 h. Second, the membrane was treated with a 3 wt% solution of H_2O_2 at 80 °C. Third, the film was soaked for 1 h in a solution of 1 M H_2SO_4 at 80 °C. Then, the membrane was purified washing three times the composite film for 1 h at 80 °C with bidistilled water.

Finally, the $\{Nafion/[(ZrO_2)\cdot(SiO_2)_{0.67}]_{\Psi_{ZrO_2}}\}$ proton conducting membranes with $0 \leq \Psi_{ZrO_2} \leq 1.79$ were hydrated in an autoclave at RH 100%, $T = 135$ °C and $P = 3.3$ bar. This later treatment was repeated twice and was considered the "reference zero point" of the thermal history of all the Nafion® composite membranes described in this report. The obtained membranes were stored in milli-Q water at room temperature inside PET bags.

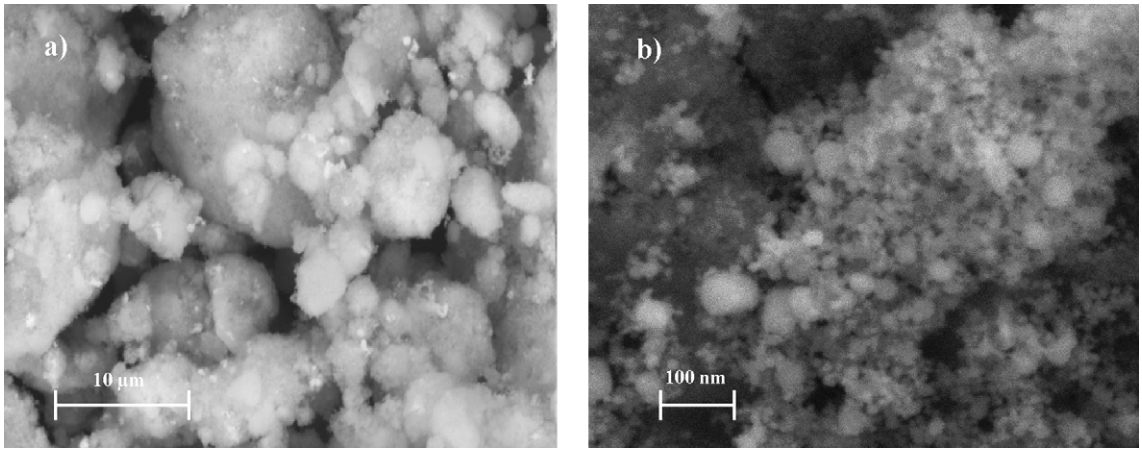

Fig. 2. SEM micrograph of pristine ZrO_2 powders (a) and FE-SEM micrograph of $[(ZrO_2)\cdot(SiO_2)_{0.67}]$ nanofiller particles (b).

Table 2
Phases composing the $[(ZrO_2)\cdot(SiO_2)_{0.67}]$ nanofiller particles determined analyzing the electron diffraction pattern of Fig. 14b)

Interplanar distances		Quality	Attribution
Measured values (Å)	Literature values (Å) [18]		
4.28	4.26	Very few spots	Traces of SiO_2
3.39	3.34	Very few spots	Traces of SiO_2
3.19	3.16	Spots	*m*-ZrO_2
2.99	2.96	Diffuse ring	*t*-ZrO_2
2.63	2.62	Spots	*m*-ZrO_2
1.83	1.83/1.82	Diffuse ring + weak spot	*t*-ZrO_2 + SiO_2
1.56	1.55	Diffuse ring	*t*-ZrO_2

2.5. Composition and proton exchange capacity (PEC) of $\{Nafion/[(ZrO_2)\cdot(SiO_2)_{0.67}]_{\Psi_{ZrO_2}}\}$ membranes

The proton exchange capacity of precursor materials and membranes was determined by titration of a heterogeneous water solution of the sample with 5 mM NaOH, using phenolphthalein as an indicator as described elsewhere [12,15]. The heterogeneous water solution of the sample was obtained by soaking the material into a NaCl 1 M water solution for 12 h. PECs of precursor materials allowed to determine Ψ_{ZrO_2}, Ψ_{SiO_2}, and Ψ which correspond to the molar ratio mol_{ZrO_2}/mol_{-SO_3H}, mol_{SiO_2}/mol_{-SO_3H} and $(mol_{ZrO_2} + mol_{SiO_2})/mol_{-SO_3H}$ (Table 1), respectively.

$\varphi = (meq_{Nafion} + meq_{ZrO_2} + meq_{SiO_2})/g_{composite}$ is the total exchange capacity of the nanocomposite membranes (Table 1) and $g_{composite}$ is the weight in grams of the materials.

2.6. Water uptake and membrane reference conditions (RC)

The water uptake of fully hydrated nanocomposite films was determined by measuring the TG profiles of the isothermal mass elimination vs. time as reported elsewhere [15]. The number of moles of water per equivalent of acid groups (λ) was determined from the isothermal TG profiles using the Eq. (1):

$$\lambda(t) = 1000\left[\frac{wt(t) - wt(t=\infty)}{wt(t=\infty)\,MW_{H_2O}\,meq/g(1 - \%wt_{ox})}\right] \quad (1)$$

where $wt(t)$ and $wt(t=\infty)$ are the weight of the membrane at $t=t$ and $t=\infty$, respectively (Fig. 1). MW_{H_2O} is the molecular weight of water; meq g^{-1} is the proton exchange capacity per 1 g of Nafion®. $\%wt_{ox}$ is the weight percentage of oxide.

WU, which corresponds to the λ value of Fig. 1 at $t=\infty$, was determined as follows. First, water was eliminated from membrane isothermally at 30 °C for 50 min. Second, the membrane was heated at 120 °C; WU and λ were measured after 80 min. The value of λ at $t=40$ min, $\lambda(t=40\,min)$, was assumed as a convenient compositional state for carrying the detailed morphological and spectroscopic characterization described in this paper. The residual water per sulfonate groups at $t=40$ min, $\lambda_{RC} = \lambda(t=\infty) - \lambda(t=40\,min)$, was assumed as the reference compositional state of membranes.

2.7. Instruments and methods

Thermogravimetric analysis was performed with a High Resolution TGA 2950 (TA Instruments) thermobalance. A working N_2 flux of 100 $cm^3\,min^{-1}$ was used. The TG profile was col-

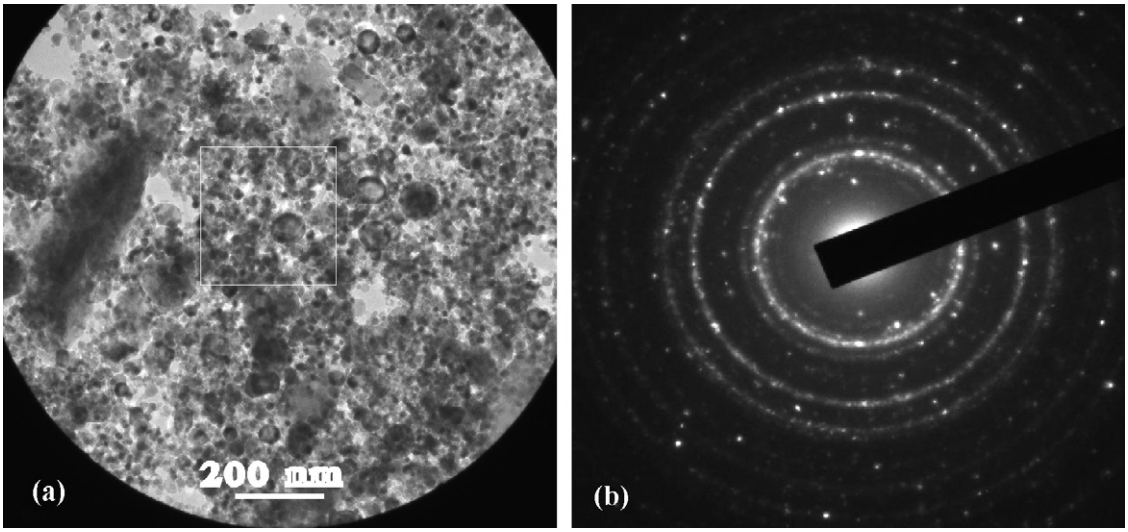

Fig. 4. TEM image of the $[(ZrO_2)\cdot(SiO_2)_{0.67}]$ nanofiller particles (the white square shows the area magnified in Fig. 3) (a), and corresponding electron diffraction pattern (b).

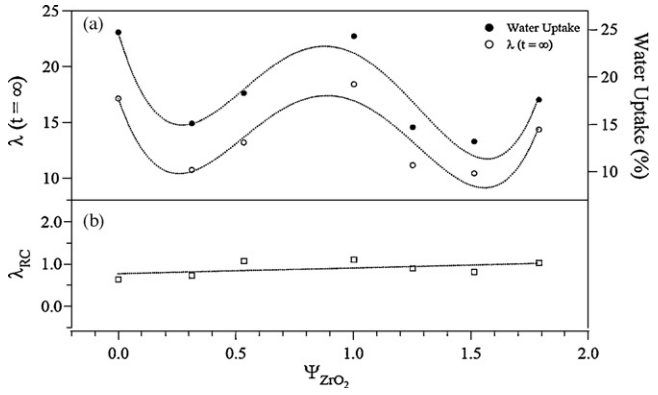

Fig. 5. Dependence on Ψ_{ZrO_2} of water uptake and: $\lambda(t=\infty)$ (a) and λ_{RC} (b). $\lambda_{RC} = \lambda(t=\infty) - \lambda(t=40\,\text{min})$.

lected in the $20 < T < 800\,^{\circ}C$ temperature range, using an open platinum pan loaded with ca. 7 mg of each material.

The morphology of the investigated samples was examined by using a Philips XL30TMP environmental scanning electron microscope (ESEM) at an acceleration voltage of 20 kV and a pressure of 0.8 torr. A vapour flow was used to eliminate the excess negative charge on the surface of the material produced by the microscope's electrons. Elemental X-ray fluorescent microanalyses were performed with an embedded EDX system coupled with an energy-dispersive X-ray spectrometer, equipped with a Si/Li detector.

Field Emission-Scanning Electron Microscopy (FE-SEM) and Energy-Dispersive X-ray analysis (EDX) were carried out on a Zeiss SUPRA 40VP instrument, equipped with an Oxford LNCA x-sight X-ray detector, operated at acceleration voltages between 5 and 10 kV.

Transmission electron microscopy (TEM) and electron diffraction (ED) were performed using a Jeol 3010 apparatus operated at 300 kV with a high-resolution pole piece (0.17 nm point-to-point resolution) and equipped with a Gatan slow-scan 794 CCD camera. Microanalyses were carried out using an Oxford Instrument EDS detector (Mod. 6636). The sample powders were suspended in isopropanol and a 5 μL drop of this suspension was deposited on a holey carbon film supported on 3 mm copper grid for TEM investigation.

FT-IR ATR spectra in the medium infrared region (MIR) were collected using a Nicolet FT-IR Nexus spectrometer equipped with a triglycine sulphate (TGS) detector at a resolution of 4 cm^{-1} and a Perkin-Elmer Frustrated Multiple Internal Reflections accessory 186-0174. FT-IR ATR measurements were obtained by averaging 1000 scans. The nanocomposite membrane was squeezed between the surface of a prismatic germanium crystal of 18 (height) × 51(width) × 2(thickness) mm^3 and a pressing counterpart device in order to achieve a perfect contact. 50% ca. of the crystal surface was covered with the membrane. An incident light angle of 45° with 25 total internal reflections was adopted. Baseline correction was performed with the Nicolet FT-IR Nexus spectrometer software.

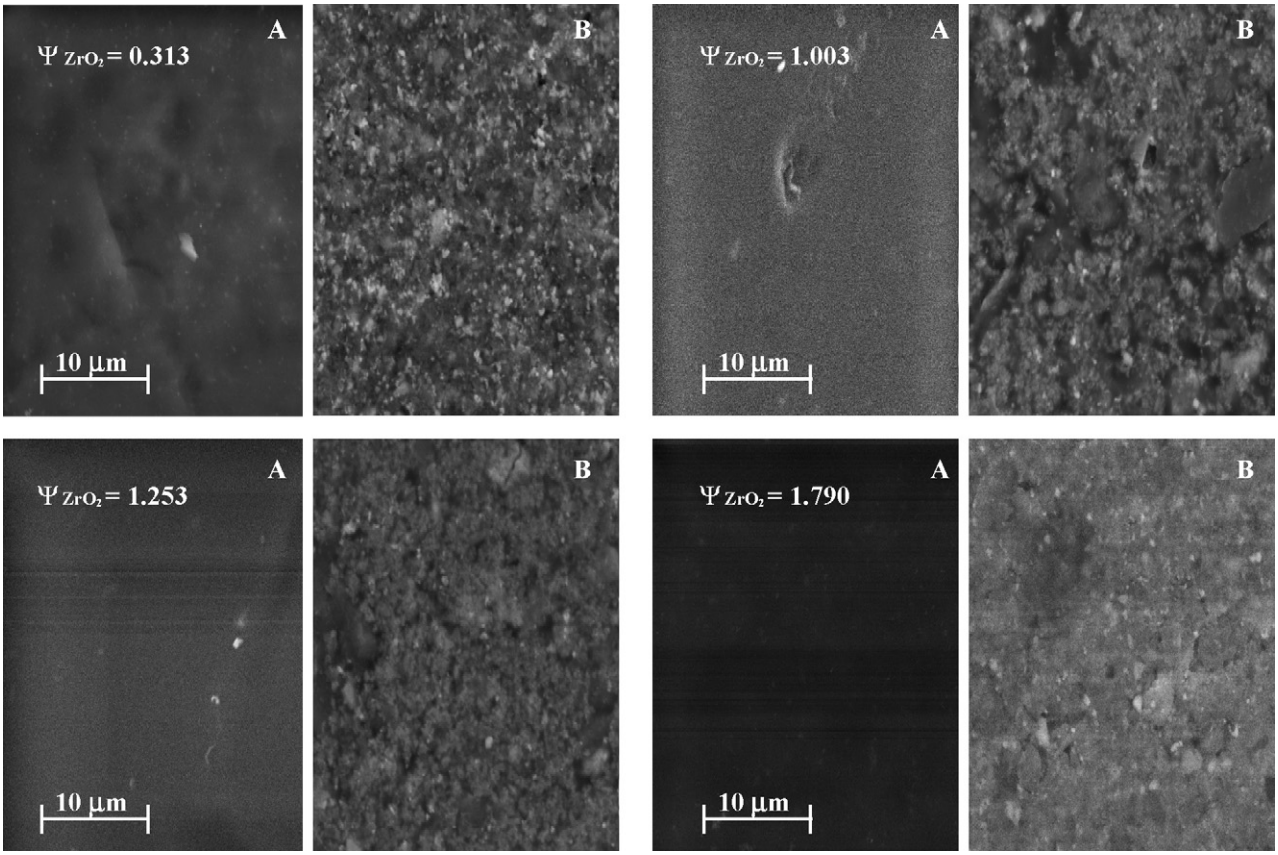

Fig. 6. SEM micrographs of selected $\{Nafion/[(ZrO_2)\cdot(SiO_2)_{0.67}]_{\Psi_{ZrO_2}}\}$ membranes with Ψ_{ZrO_2} in the range $0 \leq \Psi_{ZrO_2} \leq 1.79$. A is the upside surface of the film and B the bottom side.

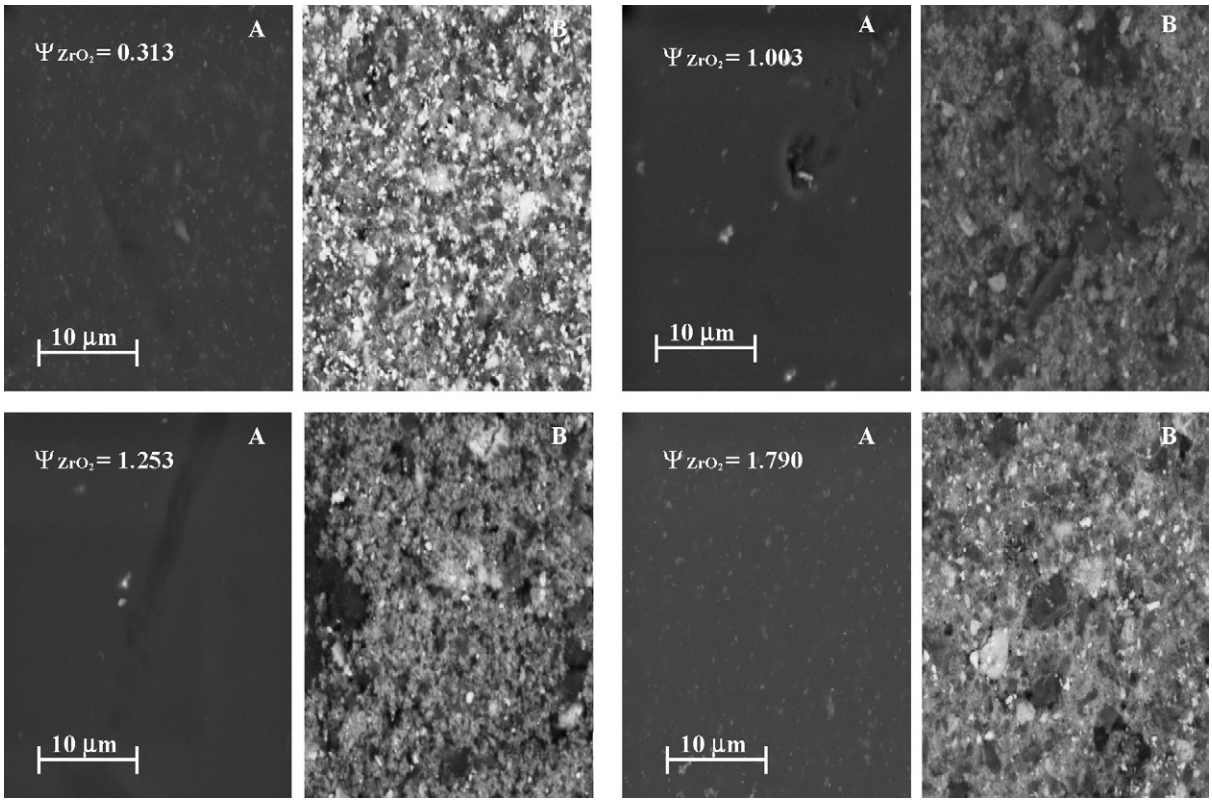

Fig. 7. Backscattered SEM images of selected $\{Nafion/[(ZrO_2)\cdot(SiO_2)_{0.67}]_{\Psi_{ZrO_2}}\}$ membranes with Ψ_{ZrO_2} in the range $0 \leq \Psi_{ZrO_2} \leq 1.79$. A is the upside surface of the film and B the bottom side.

Micro-Raman spectra were collected using a home-made instrument composed of: (a) a double Czerny Turner monochromator at a focal distance of 400 mm and a grating of 1800 lines mm^{-1} blazed at 5000 Å; (b) a Spectra-Physics Stabilite 2017 Argon Ion Laser with the excitation line set at 514.15 nm with 0.100 W, acting as the light source; (c) an Olympus BX-41 confocal microscope equipped with a 50× objective; (d) a Jobin–Yvon Symphony CCD detector system, cooled with liquid nitrogen. Each spectrum was the result of accumulation and averaging of 225 scans, collected at an integration time of 25 s.

The measurements of complex conductivity spectra were carried out in the frequency range 10 mHz–10 MHz, using a Novocontrol Alpha-A analyzer. The temperature range from 5 to 155 °C was explored by using a home made cryostat operating with a N_2 gas jet heating and cooling system. The measurements were performed using a closed home made cell. This cell allowed us to maintain the membrane wet during the measurements as follows: the freshly autoclaved membrane, sandwiched between two circular platinum electrodes, was located inside a cylindrical Teflon cell. The free volume of the cell was partially filled with 100 μL of bidistilled water in order to avoid drying during measurements up to 155 °C. The geometrical constant of the cell was determined by measuring the electrode–electrolyte contact surface and the distance between electrodes with a micrometer. No corrections for thermal expansion of the cell were carried out. The temperature was measured with accuracy greater than ±0.05 °C. The absence of water loss during measurements was checked by weighting the closed cell before and after measurements. The complex impedance ($Z(\omega)$) was converted into complex conductivity ($\sigma^*(\omega) = \sigma'(\omega) + i\sigma''(\omega)$) using the equation $\sigma^*(\omega) = k\cdot[Z^*(\omega)]^{-1}$ ($Z^*(\omega) = Z'(\omega) + iZ''(\omega)$) where k is the cell constant in cm^{-1} and $\omega = 2\pi f$ (f = frequency in Hz). The bulk conductivity of the materials, σ_{DC}, was determined by measuring the conductivity value interpolated in the plateau of the $\sigma'(\omega)$ profiles at frequencies higher than 10^5 Hz, as described elsewhere [12,17].

3. Results and discussion

3.1. Preparation of $[(ZrO_2)\cdot(SiO_2)_{0.67}]$ nanofiller

Among the additives M_xO_y, with M = Si, Ti, Zr, Hf, Ta and W, recently investigated [15], the most promising composite membranes were obtained using as M_xO_y nanofillers with M = Hf and W. It was reported that M_xO_y influences the properties of the composite materials owing to the formation of strong dynamic cross-links, $R{-}SO_3H\cdots M_xO_y\cdots HSO_3{-}R$, which improve the mechanical, thermal and dynamic characteristics of Nafion® host polymer [12,15]. In this report, to promote the interactions between nanofiller particles and the Nafion® polymer, ZrO_2 nanopowders were mixed with 25 wt% of SiO_2 fumed in solvent DMF and the suspension thus obtained was milled for 10 h with a planetary ball mill. The milling process allowed us to synthesize nanoparticles composed of a core of ZrO_2 covered by a thin layer of SiO_2. This reaction occurred thanks to the difference in Mohs hardness of the used nanopowders, 8.5 and 7 for ZrO_2 and SiO_2 fillers, respectively; and to the different acid–base characteristics

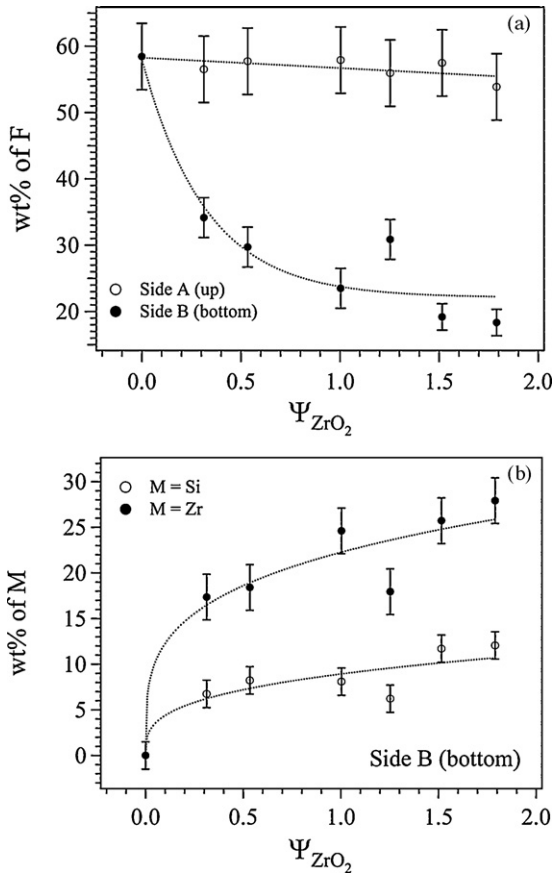

Fig. 8. SEM X-ray fluorescence analyses with energy dispersive spectroscopy (XRD-EDS) performed on different areas of A and B surfaces of $\{\text{Nafion}/[(ZrO_2)\cdot(SiO_2)_{0.67}]_{\Psi_{ZrO_2}}\}$ membranes. Dependence of: fluorine percentage (a), Si and Zr percentage (b) on Ψ_{ZrO_2}. A is the upside surface of the film and B the bottom side.

of ZrO_2 and SiO_2 materials. Fig. 2 shows the SEM and FE-SEM images of ZrO_2 powder (a) and $[(ZrO_2)\cdot(SiO_2)_{0.67}]$ nanofillers (b), respectively. Results indicated that after milling process, nanometric particles consisting of ZrO_2 oxoclusters covered by SiO_2 were obtained. This hypothesis is further supported by inspecting the TEM images and SEM micrographs of the nanopowders. The TEM micrograph shown in Fig. 3 confirms that the diameters of the final particles range from 15 to 50 nm. Furthermore, in order to gain an insight into the different phases characterizing the nanofiller material, the electron diffraction pattern (see Fig. 4b) was measured on the sample area reported in Fig. 4a. The analysis of the diffraction pattern shown in Fig. 4b indicates that the nanofiller is composed of the crystalline phases summarized in Table 2 [18]. In particular, ZrO_2, which is present as tetragonal (t-ZrO_2), and monoclinic (m-ZrO_2) zirconia, is the dominant component, whereas only very few spots attributable to quartz were revealed. These evidences witness that only very few isolated quartz nanoparticles are present in the nanopowders. EDX microanalysis performed on different areas of the TEM micrograph confirmed the information obtained by the electron diffraction pattern. Indeed, no significant amount of silicon was detected (data not shown) within the detection limit of this method. The analysis of the composition of the nanofillers was completed carrying out EDX microanalyses of the same sample in the SEM. The semiquantitative analyses thus determined indicated clearly that on the nanofiller surface, silicon is present with a Zr/Si ratio very close to the value expected on the basis of the relative amounts of reagent oxides. Taken together, the microanalysis performed with TEM indicates that (a) the analysis of electron diffraction pattern was not able to reveal silicon, probably owing to the reduced thickness of the SiO_2 interacting with the incoming electron beam; (b) the EDX measurements showed only a negligible concentration of silicon atoms. On the other hand, EDX measurements performed on SEM analyse a much larger volume of the sample, thus allow-

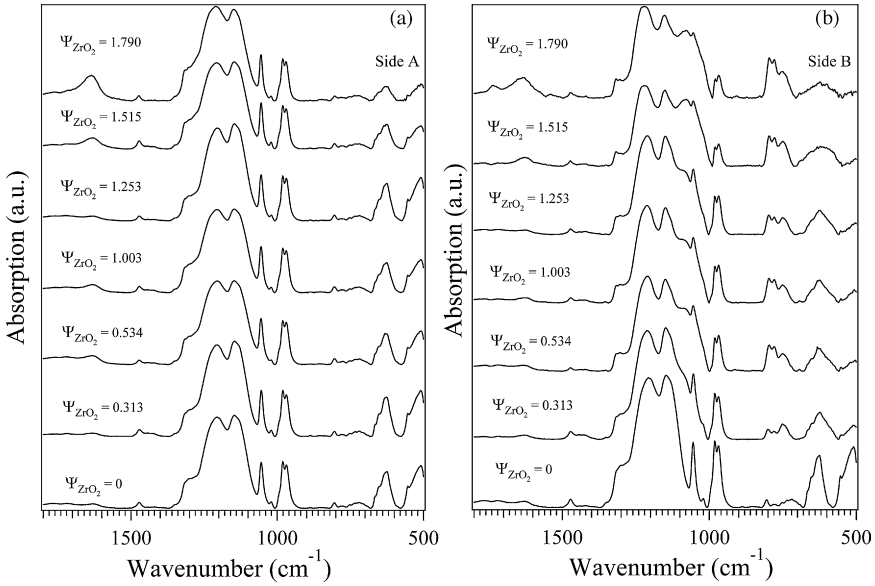

Fig. 9. FT-IR ATR absorption spectra of A (a) and B side (b) of $\{\text{Nafion}/[(ZrO_2)\cdot(SiO_2)_{0.67}]_{\Psi_{ZrO_2}}\}$ membranes with $0 \leq \Psi_{ZrO_2} \leq 1.79$. A is the upside surface of the film and B the bottom side.

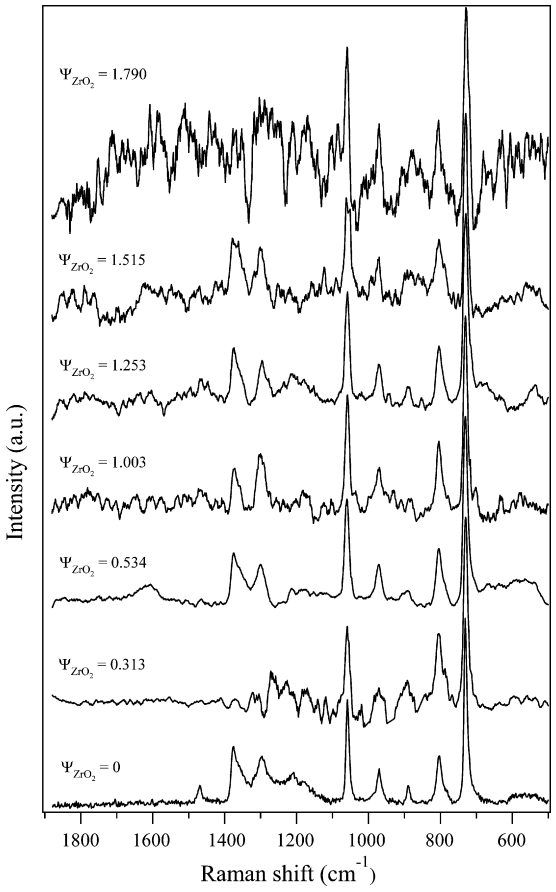

Fig. 10. MicroRaman spectra of side A of $\{Nafion/[(ZrO_2)\cdot(SiO_2)_{0.67}]_{\Psi_{ZrO_2}}\}$ membranes with $0 \le \Psi_{ZrO_2} \le 1.79$.

ing to detect efficiently the silicon atoms irrespectively of their position and distribution. In conclusion, the above morphological and micro-analytic results suggest that silicon is distributed as a very thin amorphous shell of SiO_2 around ZrO_2 grains. It is expected that such an amorphous shell of SiO_2 does not contribute significantly to the electron diffraction pattern of the nanofiller sample.

3.2. Water uptake and morphology

Fig. 1 shows the dependence of λ vs. t determined using the isothermal thermogravimetric curves, as described in Section 2. It should be noted that the curves of Fig. 1 were measured fixing the temperature at 30 and 120 °C in the range 0–50 min and 50–90 min, respectively. The isothermal mass elimination vs. t was collected on fully hydrated $\{Nafion/[(ZrO_2)\cdot(SiO_2)_{0.67}]_{\Psi_{ZrO_2}}\}$ nanocomposite films. The dependence of WU and $\lambda(t=\infty)$ on Ψ_{ZrO_2} shown in Fig. 5, was measured in the profiles of Fig. 1 at $t = 80$ min. Fig. 5 reveals that the WU and $\lambda(t=\infty)$ values of $\{Nafion/[(ZrO_2)\cdot(SiO_2)_{0.67}]_{\Psi_{ZrO_2}}\}$ membranes are lower or close to that of pristine Nafion®. In addition, WU and $\lambda(t=\infty)$ increase in the range $0.3 \le \Psi_{ZrO_2} \le 1.003$, and decrease in the range $1.003 \le \Psi_{ZrO_2} \le 1.515$. This behaviour indicates that the density of dynamic cross-links $[(ZrO_2)\cdot(SiO_2)_{0.67}]$-polymer chains: (a) in the region $0.3 \le \Psi_{ZrO_2} \le 1.003$, is higher at low nanofiller concentration and decreases as Ψ_{ZrO_2} increases; (b) in the region $1.003 \le \Psi_{ZrO_2} \le 1.515$, increases as Ψ_{ZrO_2} increases. In accordance with previous studies [15] an increase in the concentration of dynamic cross-links corresponds to a decrease in the swelling ability of the materials and thus to their water desorption event, which reduces the WU and the λ of $\{Nafion/[(ZrO_2)\cdot(SiO_2)_{0.67}]_{\Psi_{ZrO_2}}\}$ films. The water elimination rate, which is represented by the slope of λ profiles vs. time (Fig. 1), presents on Ψ_{ZrO_2} the same behaviour of $\lambda(t=\infty)$ and WU. Indeed, the highest water elimination rate is observed for the samples with $\Psi ZrO_2 = 1.003$ and $\Psi ZrO_2 = 1.79$, while the lowest values are measured for the membranes with $\Psi_{ZrO_2} = 0.313$ and $\Psi_{ZrO_2} = 1.515$. The dependence of λ_{RC} on Ψ_{ZrO_2} indicates that λ_{RC} is quite independent on the membrane composition ($\lambda_{RC} \approx 1$ for all Ψ_{ZrO_2}, Fig. 1b). In accordance with previous results [15], λ_{RC} was assumed as the reference compositional state to carry out reproducible SEM and vibrational spectroscopic investigations.

Results indicate that the density of dynamic cross-links [oxocluster]-[Nafion® host polymer] are crucial in the regulation of WU and in the water adsorption–elimination processes in $\{Nafion/[(ZrO_2)\cdot(SiO_2)_{0.67}]_{\Psi_{ZrO_2}}\}$ materials.

The morphology of $\{Nafion/[(ZrO_2)\cdot(SiO_2)_{0.67}]_{\Psi_{ZrO_2}}\}$ composite materials was investigated by SEM measurements. The selected secondary electron micrographs reported in Fig. 6 clearly indicate that the compositions of membranes are not homogeneous. Indeed A (the upside of the film after the casting procedure), presents a lower nanofiller concentration with respect to B side (the bottom side of the membrane). Furthermore, A exhibits a very smooth surface while B presents a rough surface. The backscattered images shown in Fig. 7 confirm these results and reveal that the nanofiller particles in B form a foam-like inorganic structure embedded into the bulk Nafion® host polymer. In this way, SEM microscopy allows us to hypothesize that percolation pathways with macro and micro porosities suitable for proton conduction are generated

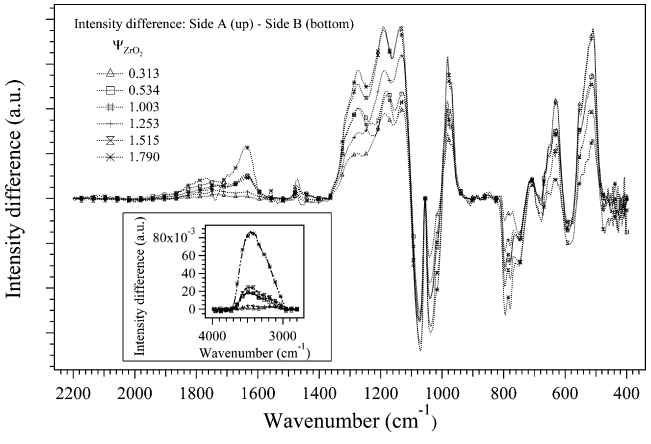

Fig. 11. Difference spectra of $\{Nafion/[(ZrO_2)\cdot(SiO_2)_{0.67}]_{\Psi_{ZrO_2}}\}$ membranes with $0 \le \Psi_{ZrO_2} \le 1.79$. Each spectrum is the result of the substraction of the FT-IR ATR spectrum of side B from that of side A shown in Fig 7. The spectra were normalized to the intensity peaking at 1055 cm^{-1}.

in B. The porosity of $\{Nafion/[(ZrO_2)\cdot(SiO_2)_{0.67}]_{\Psi_{ZrO_2}}\}$ membranes with $\Psi_{ZrO_2} = 1.003$ and 1.790 is lower than that of the other samples. Semiquantitative information on the distribution of nanofillers in A and B side was obtained by X-ray fluorescence analysis with energy-dispersive spectroscopy (XRF-EDS), performed on different areas of the composite membrane surfaces. As Ψ_{ZrO_2} increases, the percentage of fluorine atoms decreases slightly in side A and steeply in side B, thus indicating that Nafion® is distributed asymmetrically along the depth profile of the membrane (Fig. 8a). The asymmetric distribution of Nafion® between A and B side increases as Ψ_{ZrO_2} rises. These results are confirmed by analyzing the dependence in side B of the atomic percentage of both Si and Zr atoms on Ψ_{ZrO_2} (Fig. 8b). Results indicate that as Ψ_{ZrO_2} increases, the atomic ratio Si/Zr remains quite constant, while the absolute concentration of both elements increases asymptotically.

This evidence demonstrates that the porous foam-like nanofiller network structure, which is interpenetrated in bulk Nafion® membranes: (a) becomes thicker and much denser as Ψ_{ZrO_2} increases; (b) provides an inorganic network consisting of interacting $[(ZrO_2)\cdot(SiO_2)_{0.67}]$ nanoparticles which is able to stabilize mechanically and chemically the composite membrane and to increase its proton conductivity.

3.3. Vibrational spectroscopy studies

Vibrational studies were performed in order to obtain information on the secondary structure of Nafion® in $\{Nafion/[(ZrO_2)\cdot(SiO_2)_{0.67}]_{\Psi_{ZrO_2}}\}$ membranes and to study the interactions occurring between the various components of the materials. Furthermore, the structural characteristics of the A and B sides of the membranes were investigated by collecting their FT-IR ATR spectra and by analyzing in detail the resulting difference spectra. The FT-IR ATR spectra of side A and B are shown in Fig. 9a and b, respectively. The micro-Raman spectra of side A are reported in Fig. 10. It should be noted that it was impossible to acquire the micro-Raman spectra of the side B owing to the strong fluorescence of the samples. The vibrational spectra present various features which are directly correlated with the vibrational modes of: (a) the polytetrafluoroethylene (PTFE) backbone component of the hydrophobic domain of Nafion® (CF regions in the ranges 1377–1170 and 792–500 cm^{-1} [12]); (b) the polyether side chain vibrations in the region 993–950 cm^{-1}; (c) the $-SO_3H$ acid group vibrations; and d) the vibrational modes of water species embedded in bulk $\{Nafion/[(ZrO_2)\cdot(SiO_2)_{0.67}]_{\Psi_{ZrO_2}}\}$ systems [15].

A detailed analysis of the CF spectral region, carried out as reported elsewhere [19], allowed us to reveal that at room temperature the hydrophobic PTFE domains of Nafion® are composed of a mixture of polymer chains with 15_7 and 10_3 helical conformation geometries [15].

The assignment of vibrational peaks is summarized in Table 3 and was carried out correlatively on the basis of studies reported elsewhere [12,15,20].

The compositional and structural differences existing between A and B sides were investigated by analyzing the

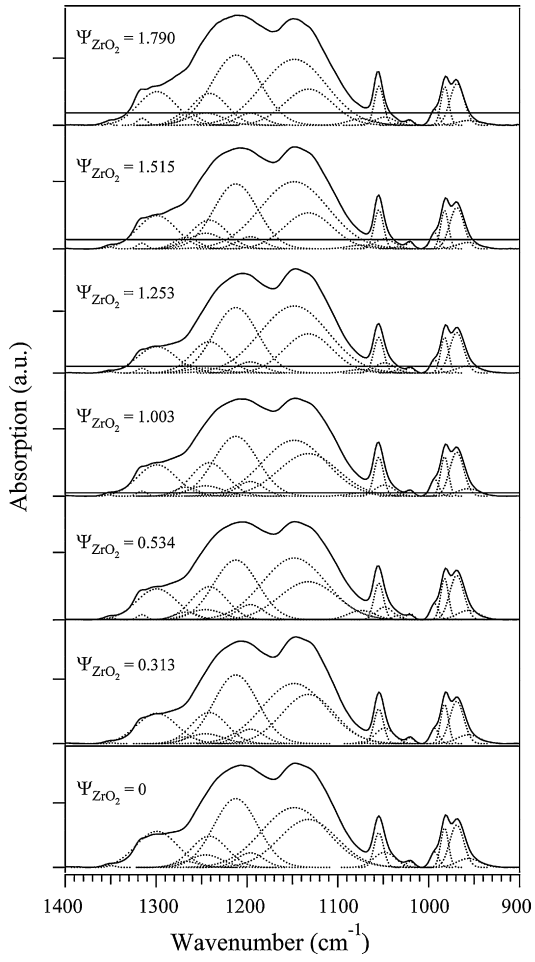

Fig. 12. Decomposition by Gaussian functions of the Mid FT-IR ATR spectra from 1400 to 900 cm^{-1} of side A of $\{Nafion/[(ZrO_2)\cdot(SiO_2)_{0.67}]_{\Psi_{ZrO_2}}\}$ membranes with $0 \le \Psi_{ZrO_2} \le 1.79$.

difference spectra obtained by subtracting the FT-IR ATR spectrum of side B from that of side A after normalization of both profiles to the band peaking at 1055 cm^{-1} (Fig. 11). Results indicated that the bands in the CF region peaking at 1132, 1196, 1245 and 1316 cm^{-1}, corresponding to the 10_3 helical conformation of fluorocarbon chains, depend on Ψ_{ZrO_2} and are more intense in side A of membranes. The absorption peaking at 1021 and 1049 cm^{-1} were assigned to the antisymmetric and symmetric stretching vibration, ν(Si–O–Si), of the silica component [20]. In accordance with SEM XRF-EDX analyses, these bands are more intense in side B. Thus, the higher concentration of $[(ZrO_2)\cdot(SiO_2)_{0.67}]$ oxocluster in B is confirmed. The fraction of each type of PTFE chain conformation present in side A was determined by the formula $\rho = A(1245)/[A(1245)+A(1212)]$, where $A(1245)$ and $A(1212)$ are the band areas of the CF_2 antisymmetric stretching vibrations of A_2 specie of fluorocarbon chains with helical conformation 10_3 and 15_7, respectively [15]. Band areas were evaluated by decomposition with Gaussian functions of the CF region of the membranes (Fig. 12). Results depicted in Fig. 13 reveal that in the hydrophobic domains found on side A of Nafion®: (a) the percentage of fluorocarbon chains with 10_3 helical

Table 3
FT-IR ATR and micro-Raman Band assignments of {Nafion/$[(ZrO_2)\cdot(SiO_2)_{0.67}]_{\Psi_{ZrO_2}}$} membranes

Observed frequencies (cm^{-1}) [a]														SC [b]	Band assignments [c,d]
Ψ_{ZrO_2}=0		Ψ_{ZrO_2}=0.313		Ψ_{ZrO_2}=0.534		Ψ_{ZrO_2}=1.003		Ψ_{ZrO_2}=1.253		Ψ_{ZrO_2}=1.515		Ψ_{ZrO_2}=1.790			
ATR	Raman	ATR	Raman	ATR	Raman	ATR	Raman	ATR	Raman	ATR	Raman	ATR	Raman		
509(m)		509(m)	509(vw)	507(w)		509(w)		509(m)		509(w)		509(vw)		E_1	helix 15_7 : $\nu_s[CF_2(17)]$; δ[FCF(68)]
627(m)		627(m)		627(w)		627(w)		627(w)		627(w)		625(vw)		E	helix 10_3 : ν[CF];δ[CCF];ν[CC]
665(sh)		665(sh)		665(sh)		665(sh)		665(sh)		665(sh)		665(sh)		A_2	helix 15_7 : δ[CCF(85)]
732(vw)	731(vs)	734(vw)	731(vs)	734(vw)	731(vs)	732(vw)	730(vs)	732(vw)	729(vs)	734(vw)	731(vs)	736(vw)	730(vs)	A_1	helix 15_7 : $\nu[CF_2(76)]$
780(vw)		781 (vw)	787(vw)	780(vw)	787(sh)	781(vw)	780(vw)	783(vw)	787(sh)	783(vw)	789(vw)	781(vw)			helix 10_3 : $\nu[CF_2]$
804(vw)	802(w)	804(vw)	804(w)	804(vw)	804(w)	804(vw)	804(w)	804(vw)	804(w)	804(vw)	804(w)	804(vw)	805(w)		ν[CS]
956(vw, b) 969(*m*)	970(w)	956(vw, b) 969(*w*)	971(vw)	956(*vw, b*) 969(*m*)	971(w)	956(*vw, b*) 969(*m*)	970(vw)	956(*vw, b*) 969(*w*)	970(vw)	956(*vw, b*) 969(*m*)	970(w)	956(*vw, b*) 969(*w*)	970(w)		ν_s[C-O-C]
983(*w*) 993(*vw*)		983(*w*) 993(*vw*)		983(*m*) 993(*vw*)		983(*m*) 993(*vw*)		983(*w*) 993(*vw*)		983(*w*) 993(*vw*)		983(*w*) 993(*vw*)			ν_{as}[C-O-C]
1021(*vw*) 1049(*vw*)		1021(*vw*) 1049(*vw*)		1021(*vw*) 1049(*vw*)		1021(*vw*) 1049(*vw*)		1021(*vw*) 1049(*vw*)		1021(*vw*) 1049(*vw*)		1021(*vw*) 1049(*vw*)			ν[Si-O-Si]
1055(w)	1059(m)	1055(w)	1059(m)	1055(w)	1059(m)	1055(w)	1058(m)	1055(w)	1058(m)	1055(w)	1061(m)	1055(w)	1059(s)		$\nu_s[.SO_3^-]$
1132(m)		1132(m)		1132(w)		1132(m)		1132(w)		1132(w)		1132(w)		E	helix 10_3 : $\nu_s[CF_2]$; δ[FCF]
1148(m)		1148(m)		1148(s)		1148(m)		1148(s)		1148(s)		1148(m)		E_1	helix 15_7 : $\nu_s[CF_2(82)]$; δ[FCF(21)]
1196(vw)	1180(vw)	1196(vw)	1174(vw)	1196(vw)		1196(vw)	1181(vw)	1196(vw)		1196(vw)		1196(vw)		E	helix 10_3 : $\nu_s[CF_2]$
1212(s)		1212(s)		1212(s)		1212(s)		1212(s)		1212(s)		1212(s)		A_2	helix 15_7 : $\nu_{as}[CF_2(112)]$
	1207(vw)		1214(sh)		1213(vw)				1213(vw,b)		1218(vw)			E_2	helix 15_7 : $\nu_{as}[CF_2(111)]$
1241(w)		1241(w)		1241(w)		1241(w)		1241(w)		1241(w)		1241(w)		A_2	helix 15_7 : $\nu_{as}[CF_2(112)]$
1245(vw)		1245(vw)		1245(vw)		1245(vw)		1245(vw)		1245(vw)		1245(vw)		A_2	helix 10_3 : $\nu_{as}[CF_2]$
1267(vw)		1267(vw)	1270(vw)	1267(vw)		1267(vw)		1267(vw)	1278(vw)	1267(vw)		1267(vw)		E	helix 10_3 : $\nu_{as}[CF_2]$
1299(w)	1296(w)	1299(w)	1305(vw)	1299(w)	1300(vw)	1299(w)	1300(w)	1299(w)	1296(w)	1299(w)	1300(w)	1299(w)		E_1	helix 15_7 : ν[CC(118)]
				1316(vw)		1316(vw)		1316(vw)		1316(vw)	1317(vw)	1316(vw)		B_1	helix 10_3 : ν[CC]
		1349(vw)		1349(vw)		1352(vw)		1352vw)		1352(vw)	1348(sh)	1352(vw)		E_2	helix 15_7: ν[CF(42)],δ[FCF(20)]; δ[CCC(43)];ν[CC(40)]
	1375(w)		1371(vw)		1375(w)		1372(vw)		1374(w)		1379(w)			A_1	helix 15_7: ν[CF(39)],δ[FCF(19)]; δ[CCC(45)];ν[CC(44)]
1471(vw)	1470(vw)	1471(vw)		1471(vw)	1464(vw)	1471(vw)	1472(vw)	1471(vw)	1469(vw)	1472(vw)	1469(vw)	1473(vw)		A_1	helix 15_7 : 2*$\nu[CF_2(76)]$
1548(vw)	1547(vw)														$\delta([H_2O]_2)$
				1558(vw)		1559(vw)		1559(vw)		1559(vw,b)		1559(vw)			$\delta([(ZrO_2)\cdot(SiO_2)_{0.65}]\cdots(H_2O)_n)$ (IV)
1633(vw)		1632(vw)		1632(vw)		1631 vw)		1630(vw)		1632(vw)		1634(w)			$\delta((H_2O)_n)$ (III)
1681(vw)		1680(vw)		1680(vw)		1680(vw)		1680(vw)		1680(vw)		1680(vw)			$\delta(H_3O^+\cdots(H_2O)_n)$ (II)
		1719(vw)		1719(vw)		1719(vw)		1719(vw)		1719(vw)		1719(vw)			$\delta([(ZrO_2)(SiO_2)_{0.65}\cdot H]^+\cdots SO_3\text{-})\cdot(H_2O)_n)$ (II')
1755(vw)		1769(vw)		1769(vw)		1769(vw)		1769(vw)		1769(vw)		1769(vw)			$\delta([H_3O^+\cdots SO_3\text{-}]\cdot(H_2O)_n)$ (I)
		1781(vw,b)		1781(vw,b)		1781(vw.b)		1781(vw,b)		1781(vw,b)		1781(vw,b)			$\delta([[(ZrO_2)\cdot(SiO_2)_{0.65}]\cdots H_3O^+\cdots SO_3\text{-})\cdot(H_2O)_n)$ (I')
3076(vw)		3071(vw)		3086(vw)		3086(vw)		3086(vw)		3086(vw)		3086(vw)			$\nu_{as}(H_3O^+)$ (I)
3155(vw)		3188(vw)		3208(vw)		3208(vw)		3208(vw)		3208(vw)		3208(w)			$\nu_{lib}(H_2O)$ (II)
3448(vw)		3470(vw)		3437(vw)		3437(vw)		3437(vw)		3437(w)		3437(m)			$\nu_s(\text{-}CF_2\cdot\cdot H_2O\cdot\cdot F_2C\text{-})$ (III)
3564(vw)		3564(vw)		3568(vw)		3568(vw)		3568(vw)		3568(vw)		3568(vw)			$_{as}(\text{-}CF_2\cdot\cdot H_2O\cdot\cdot F_2C\text{-})$ (IV)

(a) Relative intensities of observed bands are reported in parentheses: vs, very strong; s, strong; m, medium; w, weak; vw, very weak; b, broad; sh, shoulder; (b) SC is the symmetry class; (c) ν, stretching; δ, bending; ω, wagging; *t*, twisting; *r*, rocking; as, antisymmetric mode; s, symmetric mode, (d) assignment carried out correlatively as described in [12,15,20].

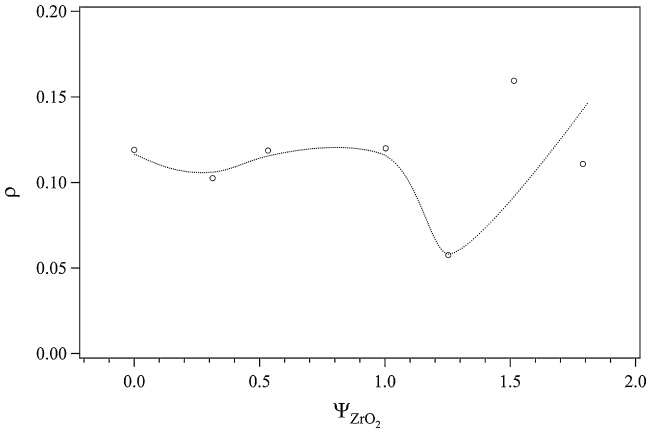

Fig. 13. ρ vs. Ψ_{ZrO_2} for $\{Nafion/[(ZrO_2)\cdot(SiO_2)_{0.67}]_{\Psi_{ZrO_2}}\}$ membranes with $0 \le \Psi_{ZrO_2} \le 1.79$. ρ is the fraction of fluorocarbon chains with 10_3 helical conformations in hydrophobic domains of Nafion®. $\rho = A(1245)/[A(1245) + A(1212)]$. A(1245) and A(1212) are the band areas of the absorption peaks at 1245 and 1212 cm^{-1}, respectively.

conformation is ranging from 6 to 16%; (b) the fluorocarbon chains with conformation 15_7 predominate; (c) in the range $0.313 \le \Psi_{ZrO_2} \le 1.003$ the percentage of 10_3 chains increases vs. Ψ_{ZrO_2} and decreases from $\Psi_{ZrO_2} = 1.003$ to $\Psi_{ZrO_2} = 1.253$.

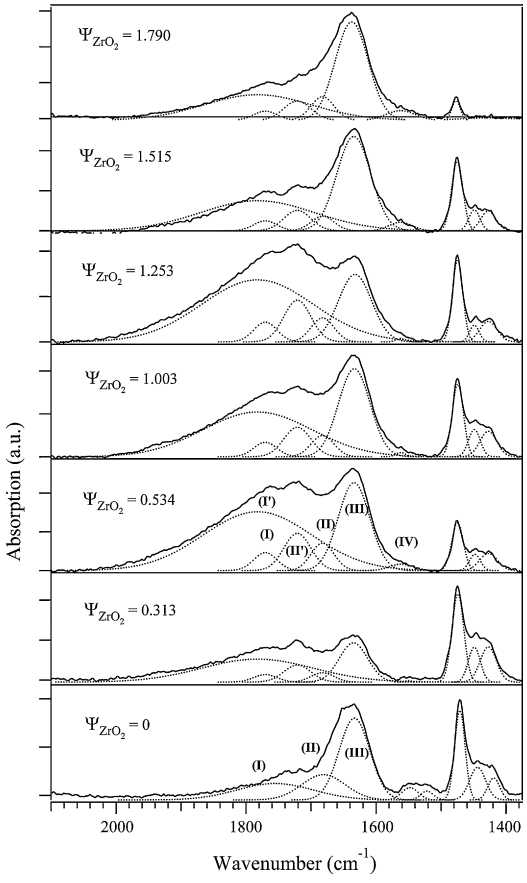

Fig. 14. Decomposition by Gaussian functions of the Mid FT-IR ATR spectral range from 2200 to 1400 cm^{-1} of side A of $\{Nafion/[(ZrO_2)\cdot(SiO_2)_{0.67}]_{\Psi_{ZrO_2}}\}$ membranes with $0 \le \Psi_{ZrO_2} \le 1.79$.

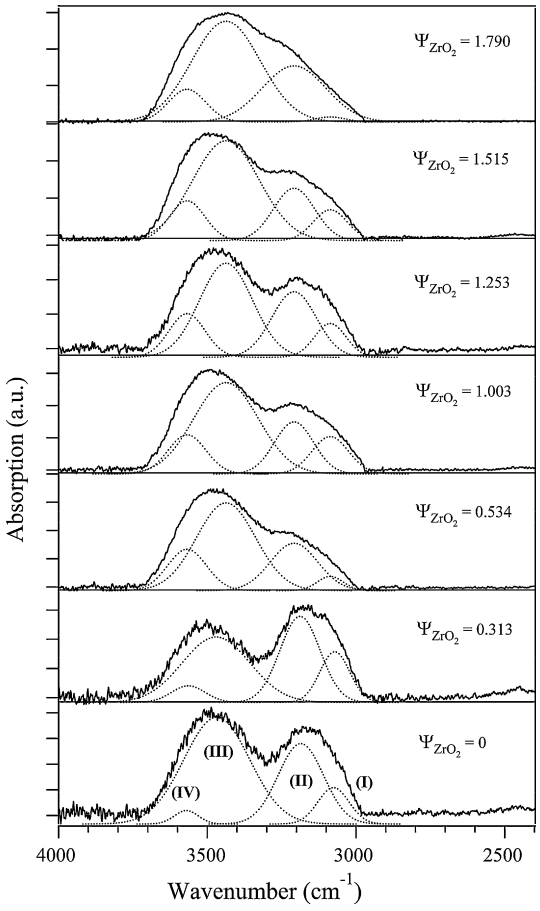

Fig. 15. Decomposition by Gaussian functions of the Mid FT-IR ATR spectral region from 4000 to 2400 cm^{-1}. Spectra of side A are shown.

It should be highlighted that this dependence on Ψ_{ZrO_2} is similar to that of water uptake shown in Fig. 5. This information reveals that: (a) WU parameter is correlated to the conformational transition $10_3 \leftrightarrow 15_7$ of fluorocarbon chains, which takes place in the PTFE hydrophobic domains of Nafion® [15]; (b) the $10_3 \leftrightarrow 15_7$ transition of fluorocarbon chains is modulated by the nanofiller concentration in membranes.

Difference spectra of $\{Nafion/[(ZrO_2)\cdot(SiO_2)_{0.67}]_{\Psi_{ZrO_2}}\}$ membranes shown in Fig. 11 indicate that polyether side chain vibrations, peaking in the region 993–960 cm^{-1}, exhibit peak profiles which are dependent on Ψ_{ZrO_2}. The water bending vibrations in the region 1590–1770 cm^{-1}, which are diagnostic for the study of the various water domains present in $\{Nafion/[(ZrO_2)\cdot(SiO_2)_{0.67}]_{\Psi_{ZrO_2}}\}$ membranes [15], were decomposed by Gaussian functions (Fig. 14). Six overlapped peaks, indicated as I, I^I, II, II^I, III and IV, compose the water bending region of Fig. 14. In accordance with previous studies [15] the four water bending vibrations indexed I, II, III and IV were assigned to the intensities peaking at 1755, 1681, 1633 and 1559 cm^{-1}, respectively. Intensity I is associated to the bending of water molecules solvating oxonium ions directly interacting with the R-SO_3^- anion groups ($\delta([H_3O^+\cdots{}^-SO_3-]\cdot(H_2O)_n)$). Peak II was attributed to modes of water molecules hydrating oxonium ions ($\delta[H_3O^+\cdots(H_2O)_n]$).

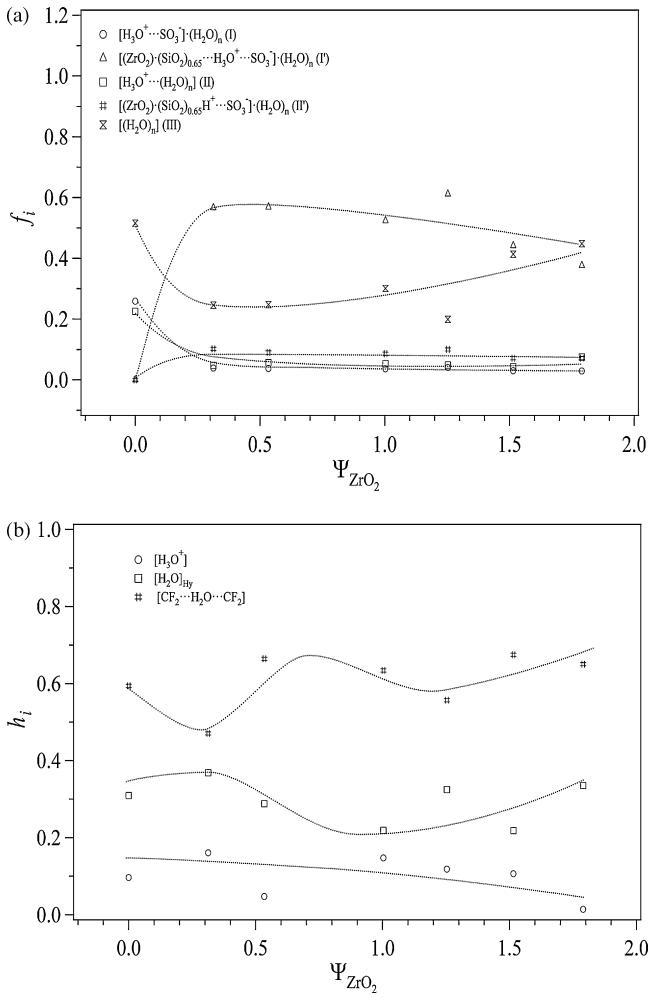

Fig. 16. f_i (a) and h_i (b) vs. Ψ_{ZrO_2} for $\{Nafion/[(ZrO_2)\cdot(SiO_2)_{0.67}]_{\Psi_{ZrO_2}}\}$ membranes. f_i is the fraction of water species present in bulk material. h_i is the fraction of water involved in hydrogen bonding networks. The semiquantitative values of f_i and h_i were determined by the formula $x_i = A_i/\sum$, where $x_i = f_i$ and h_i. A_i is the band area of peak ith. $\sum = \sum_{i=1}^{n} A_i$, and n is the number of species considered.

Peak III is attributed to bulk water $[(H_2O)_n]$, not associated with H_3O^+, and peak IV to $\delta([(ZrO_2)\cdot(SiO_2)_{0.67}]\cdots(H_2O)_n)$, the bending vibrational modes of water molecules interacting with metal oxoclusters and forming their primary hydration shell.

The intensities peaking at 1781 and 1719 cm^{-1}, singled out as I^I and II^I modes, respectively, were attributed as follows. I^I was associated to the bending vibration of water domains solvating the cross-links $[(ZrO_2)\cdot(SiO_2)_{0.67}]\cdots H_3O^+\cdots{}^-SO_3-$, $\delta(([(ZrO_2)\cdot(SiO_2)_{0.67}]\cdots H_3O^+\ldots{}^-SO_3-)\cdot(H_2O)_n)$, and II^I to the bending modes of water domains solvating the cation-anion interacting species $[(ZrO_2)\cdot(SiO_2)_{0.67}H]^+\cdots{}^-SO_3-$, $\delta([(ZrO_2)\cdot(SiO_2)_{0.67}H]^+\cdots{}^-SO_3-)\cdot(H_2O)_n)$. The investigations on water domains were completed decomposing by Gaussian functions the stretching region of water from 4000 to 2400 cm^{-1} (Fig. 15).

The intensities at 3564 and 3448 cm^{-1} were attributed to the antisymmetric (IV) and symmetric (III) ν(OH) stretching vibrations of water molecules, respectively, not involved in hydrogen bonding structures (matrix isolated molecules). The peaks at 3155 and 3076 cm^{-1} were assigned to water molecules involved in hydrogen bonding networks (II) and to the antisymmetric OH stretching vibrations of hydroxonium ions (I), respectively.

Fig. 16 (a) and (b) plot the dependence of: (a) the fraction of each type of structurally different H_2O domains, indicated as f_i, with i = I, I^I, II, II^I, III and IV; and (b) the amount of water involved in each type of detected hydrogen bonding networks, h_i with i = I, II and III, vs. Ψ_{ZrO_2}. Fig. 16(a) indicates that in $\{Nafion/[(ZrO_2)\cdot(SiO_2)_{0.67}]_{\Psi_{ZrO_2}}\}$ membranes, water is mainly involved in the solvation of the $[(ZrO_2)\cdot(SiO_2)_{0.67}]\cdots H_3O^+\cdots{}^-SO_3-$ bridges (type I^I) and as bulk water, $[H_2O]_n$ (III). The water concentration forming the solvation shell of the oxonium ions directly interacting with $R-SO_3^-$ anion groups (I) and the free oxonium ions (type II) is very low, less than 5%. 10% of total water is involved in the solvation shell of interacting bridges $(([(ZrO_2)\cdot(SiO_2)_{0.67}\cdot H]^+\cdots{}^-SO_3-)\cdot(H_2O)_n)$ (type II^I).

Finally, it should be observed that in the range $0.313 = \Psi_{ZrO_2} = 1.253$, the concentration of water in I^I domains is higher than that in (III). The dependence of h_i on Ψ_{ZrO_2} (Fig. 16b) permitted us to determine that: (a) the concentration of free hydroxonium ions in bulk materials is close to 10%; and (b) the amount of water involved in the hydrogen bonding structures $[H_2O]_{hy}$ is less than that coordinating hydroxonium ions; (c) the "isolated" water, not involved in hydrogen bonding interactions, presents the higher concentration. It should be observed that the dependence on Ψ_{ZrO_2} of the concentration of "isolated" water, presents the same behaviour of the water uptake parameter shown in Fig. 5.

Results indicate that, with respect to pristine Nafion®, the oxocluster-Nafion® side chain interactions modify significantly the distribution of water domains in bulk nanocomposite materials.

In summary, vibrational studies permitted us to conclude that the density and the strength of dynamic cross-links between $[(ZrO_2)\cdot(SiO_2)_{0.67}]$ and Nafion® play a crucial role in the modulation of: (a) the various types of water domains and their concentration in hydrophilic polar cages; and (b) the fraction of fluorocarbon chains with helical conformation 10_3 in hydrophobic PTFE domains.

3.4. Conductivity

Selected $\sigma'(\omega)$ profiles versus logarithm of frequency are shown in Fig. 17. The analysis of $\sigma'(\omega)$ curves indicates that the plateau at frequencies higher than 10^5 Hz corresponds to the σ_{DC} value of investigated samples. Thus, precise measurements of the σ_{DC} values of $\{Nafion/[(ZrO_2)\cdot(SiO_2)_{0.67}]_{\Psi_{ZrO_2}}\}$ membranes at 100% RH were determined by averaging the $\sigma'(\omega)$ values in the high frequency plateau of real component of conductivity spectra (see Section 2). The dependence of σ_{DC} on temperature (Fig. 18) confirms that the nanofiller has a significant effect on the electrical response of $\{Nafion/[(ZrO_2)\cdot(SiO_2)_{0.67}]_{\Psi_{ZrO_2}}\}$ materials. Indeed, in membranes with Ψ_{ZrO_2} in the range

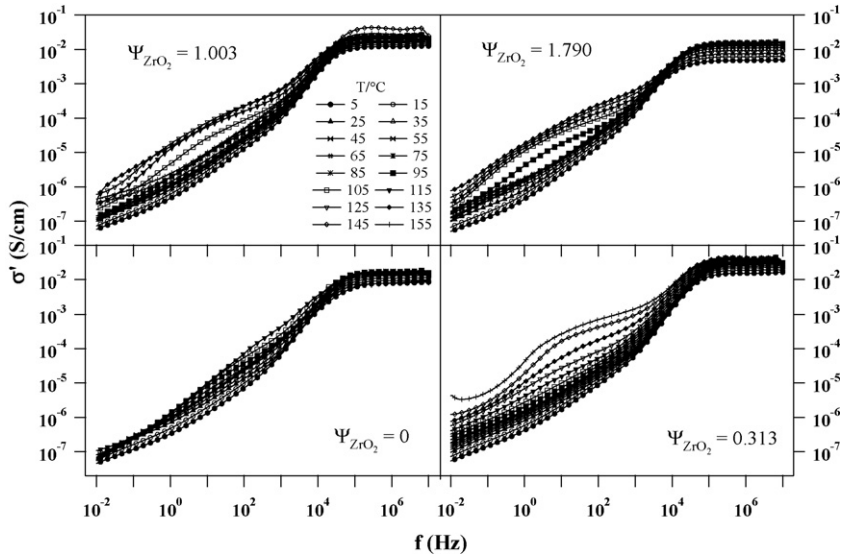

Fig. 17. Real component ($\sigma'(\omega)$) of the complex conductivity versus logf (Hz) for selected {Nafion/[$(ZrO_2) \cdot (SiO_2)_{0.67}]_{\Psi_{ZrO_2}}$} membranes.

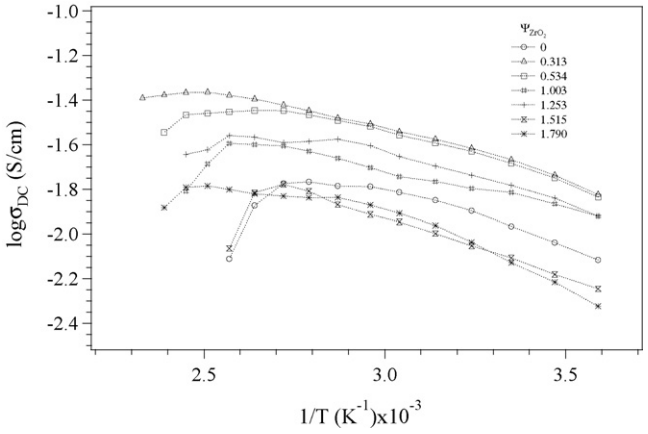

Fig. 18. Dependence of $\log\sigma_{DC}$ on temperature for {Nafion/[$(ZrO_2)\cdot(SiO_2)_{0.67}]_{\Psi_{ZrO_2}}$} membranes.

$0.313 \leq \Psi_{ZrO_2} \leq 1.253$ the conductivity is higher than that of pristine Nafion® probably owing to the fact that water concentration of I^I domains is higher than that in (III). At $\Psi_{ZrO_2} > 1.253$ a decrease of conductivity is registered, owing to a probable phase separation which originates a dilution of Nafion® bulk material. Furthermore, it should be observed that no decrease of conductivity was registered for the samples with $\Psi_{ZrO_2} = 0.313$ and 0.534 up to 135 and 115 °C, respectively. Taken together, conductivity results are in accordance with vibrational studies, thus confirming that dynamic crosslinks $[(ZrO_2)\cdot(SiO_2)_{0.67}]\cdots H_3O^+\cdots{}^-SO_3-$ between nanofiller and sulfonic acid groups play a crucial role in the modulation of conductivity and thermal stability of membranes.

4. Conclusions

In this paper is reported the preparation of six {Nafion/[$(ZrO_2) \cdot (SiO_2)_{0.67}]_{\Psi_{ZrO_2}}$} membranes with $0 \leq \Psi_{ZrO_2} \leq 1.79$. The nanofiller $[(ZrO_2)\cdot(SiO_2)_{0.67}]$ was prepared by reacting SiO_2 and ZrO_2 nanopowders suspended in a DMF solution by a ball milling process. The inorganic nanofiller exhibited a size diameter between 15 and 50 nm and consists of a ZrO_2 core covered by a layer of SiO_2. Water uptake (WU) values of {Nafion/[$(ZrO_2) \cdot (SiO_2)_{0.67}]_{\Psi_{ZrO_2}}$} membranes were: (a) lower than that of pristine Nafion®; and (b) strongly dependent on the density of dynamic crosslinks $R{-}SO_3{}^-\cdots H_3O^+\cdots[(ZrO_2)\cdot(SiO_2)_{0.67}]\cdots H_3O^+\cdots{}^-SO_3-$ present in bulk materials.

The SEM investigations revealed that the membranes are asymmetric in composition. Indeed, after the solvent casting procedure two different compositional sides were revealed. A side (the up side of the film) was richer in Nafion® while the B side (the bottom side) in nanofiller.

ESEM with EDX investigation disclosed that A side consists of a gummy and very smooth surface while B presents a rough and heterogeneous surface.

Vibrational studies, carried out by FT-IR ATR and micro-Raman spectroscopic measurements, indicate that in {Nafion/[$(ZrO_2) \cdot (SiO_2)_{0.67}]_{\Psi_{ZrO_2}}$} membranes: (a) the hydrophobic PTFE domains consist of a blend of fluorocarbon chains with helical conformation 15_7 and 10_3; (b) the concentration of 10_3 helical chains varies in the range 6–16%; (c) six different species of water domains are revealed, corresponding to: bulk water, $[(H_2O)_n]$; water solvating oxonium ions directly interacting with the $R{-}SO_3{}^-$ groups, $[H_3O^+\cdots{}^-SO_3{-}]\cdot(H_2O)_n$; acid water, $[H_3O^+\cdots(H_2O)_n]$; water molecules interacting with metal oxocluster $[(ZrO_2)\cdot(SiO_2)_{0.67}]\cdots(H_2O)_n$; water molecules involved in the solvation shell of bridges $([(ZrO_2)\cdot(SiO_2)_{0.67}]\cdots H_3O^+\cdots{}^-SO_3-)\cdot(H_2O)_n$; and water molecules solvating protonated oxoclusters directly interacting with sulfonic anion groups, $([(ZrO_2)\cdot(SiO_2)_{0.67}H]^+\cdots{}^-SO_3-)\cdot(H_2O)_n$).

It was demonstrated that in {Nafion/[$(ZrO_2)\cdot(SiO_2)_{0.67}]_{\Psi_{ZrO_2}}$} membranes water is predominantly dis-

tributed as "isolated" water and as water solvating the crosslinks $([(ZrO_2)\cdot(SiO_2)_{0.67}]\cdots H_3O^+\cdots {}^-SO_3-)\cdot(H_2O)_n$.

The conductivity studies suggest that the density of $[(ZrO_2)\cdot(SiO_2)_{0.67}]\cdots H_3O^+\cdots {}^-SO_3-$ crosslinks influences significantly both the conductivity and the thermal stability of membranes. Finally, the conductivity of $4.3\times10^{-2}\,S\,cm^{-1}$ at 135 °C and of $3.5\times10^{-2}\,S\,cm^{-1}$ at 115 °C of the $\{Nafion/[(ZrO_2)\cdot(SiO_2)_{0.67}]_{\Psi_{ZrO_2}}\}$ nanocomposite membranes with $\Psi_{ZrO_2}=0.313$ and 0.534, respectively, classify the proposed materials as promising proton conducing membranes for the application in PMFCs operating at temperatures higher than 80 °C.

Acknowledgements

Research was funded by the Italian MURST project NUME of FISR2003, "Sviluppo di membrane protoniche composite e di configurazioni elettrodiche innovative per celle a combustibile con elettrolita polimerico".

References

[1] J. Larminie, A. Dicks, Fuel Cell Systems Explained, J. Wiley and Sons, Chichester, 2000.
[2] K.A. Mauritz, R.B. Moore, Chem. Rev. 104 (2004) 4535–4585.
[3] T. Theisen, in: W. Vielstich, A. Lamm, H.A. Gasteiger (Eds.), Handbook of Fuel Cells - Fundamentals, Technology and Applications, Vol.3, John Wiley, Sons, Hoboken, New Jersey, 2003, pp. 25–38.
[4] K.A. Mauritz, Mat. Sci. Eng. C-Bio. S. 6 (1998) 121–133.
[5] G. Alberti, M. Casciola, Annu. Rev. Mater. Res. 33 (2003) 129–154.
[6] M. Neergat, K.A. Friedrich, U. Stimming, in: W. Vielstich, A. Lamm, H.A. Gasteiger (Eds.), Handbook of Fuel Cells—Fundamentals, Technology and Applications, Vol.4, John Wiley & Sons, Hoboken, New Jersey, 2003, pp. 856–877.
[7] M. Nakao, M. Yoshitake, in: W. Vielstich, A. Lamm, H.A. Gasteiger (Eds.), Handbook of Fuel Cells—Fundamentals, Technology and Applications, Vol.3, John Wiley & Sons, Hoboken, New Jersey, 2003, pp. 412–419.
[8] T.M. Thampan, N.H. Jalani, P. Choi, R. Datta, J. Electrochem. Soc. 152 (2005) A316–A325.
[9] N.H. Jalani, K. Dunn, R. Datta, Electrochim. Acta 51 (2005) 553–560.
[10] M. Aparicio, L.C. Klein, J. Electrochem. Soc. 152 (2005) A493–A496.
[11] M.B. Satterfield, P.W. Majsztrik, H. Ota, J.B. Benziger, A.B. Bocarsly, J. Polym. Sci. Pol. Phys. 44 (2006) 2327–2345.
[12] V. Di Noto, R. Gliubizzi, E. Negro, G. Pace, J. Phys. Chem. B 110 (2006) 24972–24986.
[13] K.A. Mauritz, I.D. Stefanithis, S.V. Davis, R.W. Scheetz, R.K. Pope, G.L. Wilkes, H.H. Huang, J. Appl. Polym. Sci. 55 (1995) 181–190.
[14] K.T. Adjemian, S. Srinivasan, J. Benziger, A.B. Bocarsly, J. Power Sources 109 (2002) 356–364.
[15] V. Di Noto, R. Gliubizzi, E. Negro, M. Vittadello, G. Pace, Electrochim. Acta, available online 13 May 2007.
[16] W.L.F. Armarego, D.D. Perrin, Purification of laboratory chemicals, fourth ed., Butterworth-Heinemann, Oxford, 1996, p. 19.
[17] V. Di Noto, M. Vittadello, R.P.J. Jayakody, A.N. Khalfan, S.G. Greenbaum, Electrochim. Acta 50 (2005) 4007–4014.
[18] Powder Diffraction File, JCPDS International Centre for Diffraction Data, Swarthmore PA, PDF no. 5-490 (quartz), 24-1165 (*m*-ZrO_2), 17-923 (*t*-ZrO_2).
[19] V. Di Noto, D. Longo, V. Munchow, J. Phys. Chem. B 103 (1999) 2636–2646.
[20] V. Di Noto, P. Damioli, M. Vittadello, R. Dall'Igna, F. Boella, Electrochim. Acta 48 (2003) 2329–2342.